JACS
JOURNAL OF THE AMERICAN CHEMICAL SOCIETY
Communication
pubs.acs.org/JACS

In Operando Identification of Geometrical-Site-Dependent Water Oxidation Activity of Spinel Co_3O_4

Hsin-Yi Wang,[†] Sung-Fu Hung,[‡] Han-Yi Chen,[§] Ting-Shan Chan,[∥] Hao Ming Chen,*[,‡] and Bin Liu*[,†]

[†]School of Chemical and Biomedical Engineering, Nanyang Technological University, Block N1.2, 62 Nanyang Drive, Singapore 637459, Singapore

[‡]Department of Chemistry, National Taiwan University, Taipei, 106, Taiwan, Republic of China

[§]TUM CREATE, 1 CREATE Way, #10-02 CREATE Tower, Singapore 138602, Singapore

[∥]National Synchrotron Radiation Research Center, Hsinchu 300, Taiwan, Republic of China

Supporting Information

ABSTRACT: Spinel Co_3O_4, comprising two types of cobalt ions: one Co^{2+} in the tetrahedral site (Co^{2+}_{Td}) and the other two Co^{3+} in the octahedral site (Co^{3+}_{Oh}), has been widely explored as a promising oxygen evolution reaction (OER) catalyst for water electrolysis. However, the roles of two geometrical cobalt ions toward the OER have remained elusive. Here, we investigated the geometrical-site-dependent OER activity of Co_3O_4 catalyst by substituting Co^{2+}_{Td} and Co^{3+}_{Oh} with inactive Zn^{2+} and Al^{3+}, respectively. Following a thorough in operando analysis by electrochemical impedance spectroscopy and X-ray absorption spectroscopy, it was revealed that Co^{2+}_{Td} site is responsible for the formation of cobalt oxyhydroxide (CoOOH), which acted as the active site for water oxidation.

Water electrolysis provides a promising way to supply and store clean and sustainable energy,[1−3] which consists of two half reactions: the hydrogen evolution reaction (HER) and the oxygen evolution reaction (OER).[4] Among these two reactions, water oxidation is the rate-determining step because of the thermodynamic uphill reaction that involves a stepwise four-electron transfer, which usually requires a high overpotential to drive the reaction.[5] Thus, it becomes extremely important to develop efficient OER electrocatalysts. Spinel cobalt oxide (Co_3O_4) is an earth-abundant and efficient OER catalyst with competitive activity which has been extensively studied as a replacement to noble metal-based catalysts.[6−8] It has been disclosed that the catalytic activity of Co_3O_4 is sensitively dependent on the exposed crystal facets, which could influence the adsorption/desorption of reactants/products.[9] Spinel Co_3O_4 comprises two types of geometrical cobalt ions with different oxidation states: one Co^{2+} ion in the tetrahedral site and two Co^{3+} ions in the octahedral site (denoted as Co^{2+}_{Td} and Co^{3+}_{Oh}, respectively). The population of Co^{2+}_{Td} and Co^{3+}_{Oh} on different exposed facets of Co_3O_4 nanostructures has been demonstrated as the key to influence the catalytic performance.[10,11] For example, in heterogeneous catalysis, Co_3O_4 nanorods with predominately exposed Co^{3+}_{Oh} sites showed superior catalytic activities toward CO[9,12] and ethylene oxidation.[13] In electrocatalysis, the vigorous electrochemical water oxidation of phosphate containing cobalt oxide (or Co-Pi) was ascribed to the CoO_6 octahedra geometry,[14,15] where active Co ion could be reversibly oxidized and reduced between Co(II) and Co(IV).[16,17] Meanwhile, the observed high turnover frequency (TOF) of OER on cobalt-based perovskite[18−20] and delithiated $Li_{1-x}CoO_2$[21,22] was attributable to the modified electronic states of d-orbital configuration of Co^{3+}_{Oh} species. Several previous works have proposed that the electrochemical OER performance of spinel Co_3O_4 is also geometry-site-dependent,[23−26] where Co^{3+}_{Oh} with a higher oxidation state should dominate the water oxidation reaction, yet Co^{2+}_{Td} is relatively inactive. However, the chemical environment of Co_3O_4 is contributed by both Co^{2+}_{Td} and Co^{3+}_{Oh} species, and more importantly, such environment is dynamically changeable during electrocatalysis with applied bias. Without conclusive evidence, the OER active sites in Co_3O_4 remain elusive.

To differentiate the catalytic active sites for water oxidation in spinel Co_3O_4, we separately studied the activity of Co^{2+}_{Td} and Co^{3+}_{Oh} for OER based on a simple ion-substitution strategy. Catalytically inactive Zn^{2+} and Al^{3+} with d^0 electronic configuration were used to replace Co^{2+} and Co^{3+} in their corresponding tetrahedral and octahedral sites, respectively. To disclose the real-time OER activities of substituted cobalt oxides, electrochemical water oxidation was probed in operando by electrochemical impedance spectroscopy and X-ray absorption spectroscopy. Our results indicate that Co^{2+}_{Td} and Co^{3+}_{Oh} differ from each other in surface kinetics and electrochemical reactivity toward OER and, more importantly, that Co^{2+}_{Td}, which is capable of releasing electrons under applied bias, is responsible for the formation of cobalt oxyhydroxide (CoOOH) on the Co_3O_4 surface, which acts as the main active site for OER.

Substituted cobalt oxides were prepared by a simple sol−gel method (see the Supporting Information). As displayed in Figure 1a, both zinc-substituted Co_3O_4 ($ZnCo_2O_4$) and aluminum-substituted Co_3O_4 ($CoAl_2O_4$) maintain the cubic-spinel structure, which is identical to that of pure Co_3O_4. However, the size and morphology were unavoidably influenced due to different ionic size and electronic state of foreign atoms as compared with those of the host cobalt in Co_3O_4 (see Figure 1b−d). The polyhedron-like Co_3O_4 particles are ∼100 nm in

Received: October 8, 2015
Published: December 28, 2015

DOI: 10.1021/jacs.5b10525
J. Am. Chem. Soc. 2016, 138, 36−39

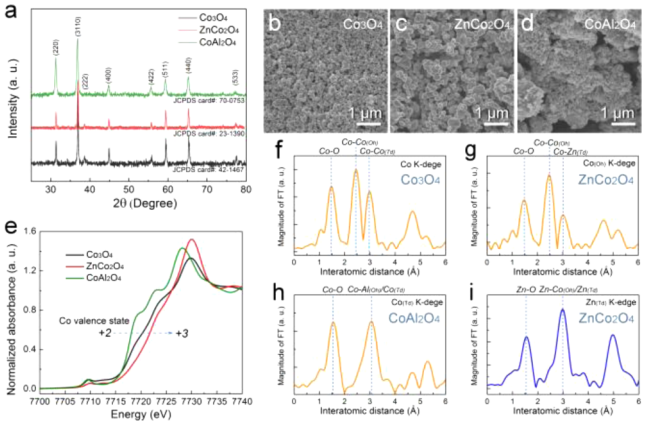

Figure 1. Structural information on substituted Co_3O_4. (a) XRD patterns and (b–d) SEM images of Co_3O_4, $ZnCo_2O_4$, and $CoAl_2O_4$. (e) Normalized ex situ Co K-edge XANES spectra, from which we could determine the Co valence states to be +2, between +2 and +3, and +3 in $CoAl_2O_4$, Co_3O_4, and $ZnCo_2O_4$, respectively. (f–h) Co K-edge EXAFS spectra for Co_3O_4, $ZnCo_2O_4$, and $CoAl_2O_4$, respectively. (i) Zn K-edge EXAFS spectrum for $ZnCo_2O_4$. The interatomic distances are shorter than the actual values owing to the fact that Fourier transform (FT) spectra were not phase corrected. Note: Enlarged version of this figure is shown in Figure S9.

diameter (Figure 1b), while the size of $ZnCo_2O_4$ and $CoAl_2O_4$ particles become larger and smaller, respectively (Figure 1c,d). The valence states of cobalt in substituted cobalt oxides were revealed using X-ray absorption near edge structure (XANES), where the position of the absorption edge could be used as an indicator. Figure 1e shows the valence state of cobalt in different Co_3O_4 samples, which follows the order of $ZnCo_2O_4$ > Co_3O_4 > $CoAl_2O_4$. This trend agrees well with our expectation that Co^{3+} was preserved in $ZnCo_2O_4$, while Co^{2+} was preserved in $CoAl_2O_4$, and an average oxidation state ($Co^{+2.67}$) of cobalt is expected for Co_3O_4. Furthermore, X-ray photoelectron spectroscopy (XPS) spectra (Figure S1) confirm the exposed metal ions: Co^{3+} on $ZnCo_2O_4$, Co^{2+} on $CoAl_2O_4$, and Co^{2+} and Co^{3+} on Co_3O_4. The structural position of various metals in substituted cobalt oxides was probed by extended X-ray absorption fine structure (EXAFS). As displayed in Figure 1f–i, the first peak at ~1.5 Å can be assigned to single scattering paths of the metal ion to the closest neighboring crystal oxygen. The second and third peaks at ~2.5 and ~3.0 Å, respectively, are attributable to the scattering paths of the metal ion to its closest neighboring metal ion in octahedral or tetrahedral site, depending on the position where the metal ion initially stays. Figure S2 illustrates a clear relationship of the interatomic distance between the two geometrical metal ions. Octahedrally coordinated cations should possess two different atom–atom bond distances (interatomic distances of ~2.5 and ~3.0 Å) from surrounding metal ions in octahedral and tetrahedral sites, respectively. On the other hand, the tetrahedrally coordinated cations only have one atom–atom bond distance of ~3.0 Å. Therefore, it is concluded that Co^{2+} in the tetrahedral site has been successfully replaced by Zn^{2+} in $ZnCo_2O_4$, while Co^{3+} in the octahedral site has been successfully replaced by Al^{3+} in $CoAl_2O_4$, and both $ZnCo_2O_4$ and $CoAl_2O_4$ still maintain the spinel structure, AB_2X_4 (A^{2+} = tetrahedral metal ion, B^{3+} = octahedral metal ion, and X = chalcogen), the same as that of spinel Co_3O_4.

The OER activities of pristine and substituted cobalt oxides were evaluated by cyclic voltammetry (CV) and linear scanning voltammetry (LSV) with corresponding Tafel plots (Figure S3). To make a fair comparison, the OER activities were normalized to the electrocatalytic active surface area as determined by double-layer capacitance (DLC) method (Figure S4). As shown in the normalized CV curves (Figure 2a), a pair of redox peaks for

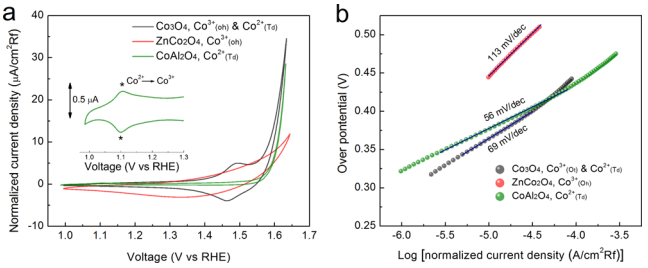

Figure 2. Electrochemical performance toward OER. (a) Normalized cycling voltammetry curves and (b) corresponding Tafel slopes for Co_3O_4, $ZnCo_2O_4$, and $CoAl_2O_4$.

Co_3O_4 at 1.49 V (anodic) and 1.47 V (cathodic) vs RHE are observable, which can be assigned to the redox couple of Co(III)/Co(IV),[27] but such a characteristic feature vanishes for $ZnCo_2O_4$, where only a typical capacitive current is observed. It was proposed that the redox process could only take place at the Co^{2+} tetrahedral sites in Co_3O_4.[25] CV curve of $CoAl_2O_4$ exhibits an almost noncapacitance feature in the voltage range between 1.0 and 1.55 V vs RHE. However, a small pair of redox peaks can still be identified at 1.13 V (anodic) and 1.10 V (cathodic) vs RHE (Figure 2a, insert), which can be attributed to the redox couple of Co(II)/Co(III) in the tetrahedral site.[28,29] A sharp rising in OER current after 1.55 V vs RHE indicates that a high overpotential is needed to trigger the reaction of water oxidation for $Co^{2+}{}_{Td}$ predominated $CoAl_2O_4$. It is interesting to find the absence of redox peak at around 1.45 V vs RHE for $CoAl_2O_4$, which is usually assigned to the Co(III)/Co(IV) couple as that in Co_3O_4. The oxidation of Co(III) at the tetrahedral site is suggested to be postponed and appears together with OER current rising due to the influence of Al substituent. A series of variation of OER currents behaving as a function of Zn and Al substituting amount are shown in Figure S6. Tafel plots (Figure 3b) obtained from the normalized polarization curves (Figure S5) reveal surface kinetic properties of OER. The general OER mechanism in alkaline solution on the metal site (M) begins with a proton-coupled electron transfer from a surface-bound aquo species followed by an O–O bond formation,[30,31] which is described as follows:

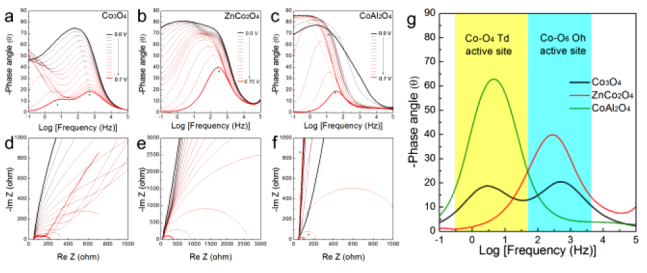

Figure 3. In operando EIS. (a–c) Phase angle vs log(frequency) plots of EIS data recorded at various voltages and (d–f) the corresponding Nyquist plots for Co_3O_4, $ZnCo_2O_4$, and $CoAl_2O_4$, respectively, where the applied voltage is referenced to SCE. (g) Phase angle vs log(frequency) plots from Co_3O_4, $ZnCo_2O_4$, and $CoAl_2O_4$ based on similar OER current densities. Note: Enlarged version of this figure is shown in Figure S10.

DOI: 10.1021/jacs.5b10525
J. Am. Chem. Soc. 2016, 138, 36–39

$$M{-}OH_2 + OH^- \rightarrow M{-}OH + H_2O + e^- \quad (1)$$

$$M{-}OH + OH^- \rightarrow M{-}O^* + H_2O + e^- \quad (2)$$

$$M{-}O^* + OH^- \rightarrow M{-}OOH + e^- \quad (3)$$

$$M{-}OOH + OH^- \rightarrow M{-}OH_2 + O_2 + e^- \quad (4)$$

Among different samples tested, $ZnCo_2O_4$ shows a Tafel slope of 113 mV/dec, indicating that the OER process in $ZnCo_2O_4$ is rate limited at the first stage where the surface of catalyst is strongly bonded with −OH groups (reaction order = 1 with respect to OH^- species with featured Tafel slope of 120 mV/dec).[32] The Tafel slopes for $CoAl_2O_4$ (~56 mV/dec) and Co_3O_4 (~69 mV/dec) are much smaller than that for $ZnCo_2O_4$ and close to a featured Tafel slope of 60 mV/dec, suggesting a different rate-determining step. The OER reactions of $CoAl_2O_4$ and Co_3O_4 are controlled by the equilibrium state between the −OH adsorption and O−O formation in an intermediate coverage regime of −OH groups on the active sites.[32]

To gain in-depth information on underlying controlling factors for water oxidation, in operando electrochemical impedance spectroscopy (EIS) measurements were carried out. The current response was measured over a frequency range from 10^5 to 10^{-1} Hz under AC perturbation voltage with a small amplitude (10 mV) superimposed on an applied DC bias.

Figure 3a−c shows the phase angle relaxation as a function of frequency in terms of various electrochemical reactions (Bode phase plot). As displayed in Figure 3a, two phase peaks in Co_3O_4 (one at middle frequency and the other at low frequency) gradually move toward each other with an increase in applied external bias. The corresponding Nyquist plot (Figure 3d) shows two semicircles at high applied potential (0.7 V vs SCE). Only one phase peak was observed in $ZnCo_2O_4$ at the middle frequency region if Co^{2+} in the tetrahedral site of Co_3O_4 was replaced by Zn^{2+} (Figure 3b), and the corresponding Nyquist plot (Figure 3e) only displays one large semicircle in the entire bias range of testing. Interestingly, if Co^{3+} in the octahedral site of Co_3O_4 was replaced by Al^{3+}, only one phase peak could be identified at the low frequency region in the Bode phase plot, which moved toward lower frequency with an increase in applied bias, opposite as compared to Co_3O_4 and $ZnCo_2O_4$. The corresponding Nyquist plot shows steep straight lines nearly perpendicular to the *x*-axis (Figure 3f) in the potential range of 0−0.55 V vs SCE, indicating infinite charge-transfer resistance. This observation is consistent with the result obtained in the CV measurement, in which almost no capacitive feature could be identified due to weak electronic interaction. When applied bias was higher than 0.55 V vs SCE, a corresponding semicircle appeared in its Nyquist plot. Figure 3g merges the relaxation curves selected from Co_3O_4 (0.6 V vs SCE), $ZnCo_2O_4$ (0.75 V vs SCE), and $CoAl_2O_4$ (0.6 V vs SCE). The relaxation curves were selected at different applied potentials based on comparable OER current densities (Figure 2b). As shown in Figure 3g, two electrochemical processes at two different frequency regions can be clearly identified: the middle frequency region (10^2−10^3 Hz) is associated with surface DLC,[33,34] and the low frequency region (10^0−10^1 Hz) should be related to the nonhomogeneous charge distribution caused by surface oxidized species (e.g., $Co^{3+} \rightarrow Co^{4+}$).[34−36] Thus, based on the EIS results, it is reasonable to deduce that $Co^{3+}{}_{Oh}$ in Co_3O_4 is responsible for surface DLC, while $Co^{2+}{}_{Td}$ is responsible for water oxidation. Our conclusion coincides well with the observation in CV and Tafel plots, where $ZnCo_2O_4$ exhibits pure capacitive behavior with strong −OH affinity, while $CoAl_2O_4$ shows weak electronic interaction followed by rising in OER current. Meanwhile, the synergistic effect of $Co^{2+}{}_{Td}$ and $Co^{3+}{}_{Oh}$ in Co_3O_4 needs to be emphasized. The −OH accumulation induced DLC should benefit the overall catalytic driving force, which could be seen from the CV curve as shown in Figure 2a. As compared with Co_3O_4, the OER onset is postponed, and the potential of redox couple of Co(III)/Co(IV) is shifted after OER current for $CoAl_2O_4$. On the other hand, the kinetics of $Co^{2+}{}_{Td}$ could also be masked by DLC,[35] as a larger Tafel slope (69 mV/dec) was observed in Co_3O_4 as compared to that of $CoAl_2O_4$ (56 mV/dec).

In operando EXAFS was performed to probe the variation of chemical environment on the catalyst during OER using a homemade in operando cell (Figure S7). Figure 4a−c displays

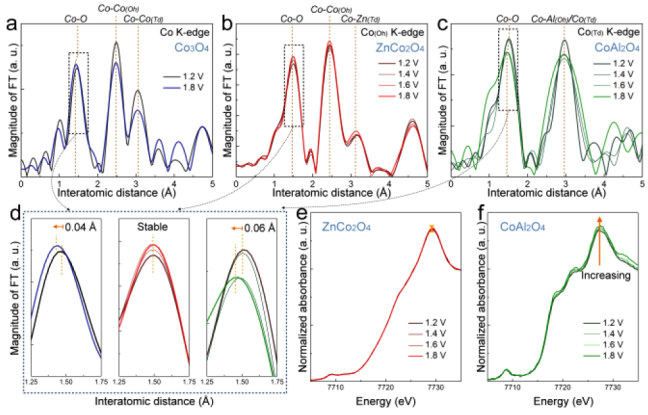

Figure 4. In operando X-ray absorption spectroscopy. (a−c) Co K-edge EXAFS spectra for Co_3O_4, $ZnCo_2O_4$, and $CoAl_2O_4$, where the applied voltage is referenced to RHE. (d) Enlarged Co K-edge EXAFS spectra on Co−O interatomic distance for Co_3O_4 (blue), $ZnCo_2O_4$ (red), and $CoAl_2O_4$ (green). (e and f) Normalized in operando Co K-edge XANES spectra for $ZnCo_2O_4$ and $CoAl_2O_4$. Note: Enlarged version of this figure is shown in Figure S11.

the Co K-edge spectra, which show that the corresponding interatomic distances of $Co^{3+}{}_{Oh}$ and $Co^{2+}{}_{Td}$ to their neighboring atoms in all catalysts remain nearly constant at the voltage range between 1.2 and 1.8 V vs RHE, indicating a highly stable bulk structure of spinel.[38] However, slightly compressed Co−O bond could still be observed in Co_3O_4 during OER (Figure 4d), indicating partial oxidation of the catalyst surface. Interestingly, the shrinking in length of Co−O bond with applied bias could only be observed on $Co^{2+}{}_{Td}$ predominated $CoAl_2O_4$, but not on $ZnCo_2O_4$ (Figure 4d). The corresponding k^3-weighting k-space spectra (Figure S8) also reveal the variation between 1.0 and 1.8 V vs RHE in Co_3O_4 and $CoAl_2O_4$. The Co K-edge EXAFS spectra (Figure 4e) show that the white line intensity remains constant for $ZnCo_2O_4$, but keeps growing up for $CoAl_2O_4$ with increase in applied positive bias (Figure 4f), indicating accumulation of positive charges on the cobalt ions on $CoAl_2O_4$, i.e., $Co^{2+}{}_{Td}$ with an initially low oxidation state is able to release electrons under applied bias, which can facilitate the interaction with oxygen intermediates on the catalyst surface. This electron-releasing and oxygen-adopting process suggests the formation of CoOOH (eq 3), which acts as the main active sites in the turnover-limiting pathway for water oxidation on Co_3O_4.[32,37] As compared with reported phosphate containing cobalt oxide (or Co-Pi), where the octahedral Co center in a cubane structure[39,14] is capable to be oxidized to Co(IV) in the OER cycle involving a chemical turnover-limiting process of

DOI: 10.1021/jacs.5b10525
J. Am. Chem. Soc. 2016, 138, 36−39

CoOOH formation,[16] our work reveals that the Co^{3+}_{Oh} species should be relatively inactive as compared to Co^{2+}_{Td} in Co_3O_4 spinel. Based on the fact of the present result, it is concluded that to form CoOOH intermediate species, the oxidation process on an active Co ion is the critical process, and Co^{2+}_{Td} is disclosed as the active species in Co_3O_4, which can be oxidized under applied anodic bias. Thus, the accumulated positive charge within the catalyst can greatly assist the CoOOH formation (eq 3) on Co_3O_4 surface.

In summary, we have successfully identified distinct kinetics and electrochemical reactivity of Co^{2+}_{Td} and Co^{3+}_{Oh} toward OER in spinel Co_3O_4. Our study showed that Co^{2+}_{Td} in Co_3O_4 is capable of releasing electrons under applied bias, promoting the affinity to oxygen ions on the catalyst surface to form CoOOH, which acted as the main active site for OER. However, the Co^{3+}_{Oh} predominated catalyst, $ZnCo_2O_4$, tended to stably bond with −OH groups, thus limiting its catalytic activity. Our work further emphasizes the importance of in operando investigations on electrocatalysis for instantaneously probing the real-time electrochemical kinetics and surface reactions.

■ ASSOCIATED CONTENT

Supporting Information

The Supporting Information is available free of charge on the ACS Publications website at DOI: 10.1021/jacs.5b10525.

Experimental methods and details (PDF)

■ AUTHOR INFORMATION

Corresponding Authors

*haomingchen@ntu.edu.tw

*liubin@ntu.edu.sg

Notes

The authors declare no competing financial interest.

■ ACKNOWLEDGMENTS

This work was supported by the Nanyang Technological University startup grant: M4080977.120, Singapore Ministry of Education Academic Research Fund (AcRF) Tier 1: M4011021.120, Singapore A*Star Science and Engineering Research Council − Public Sector Funding (PSF): M4070232.120 and the National Research Foundation (NRF), Prime Minister's Office, Singapore under its Campus for Research Excellence and Technological Enterprise (CREATE) program, and the Ministry of Science and Technology, Taiwan (contract no. MOST 104-2113-M-002-011-MY2).

■ REFERENCES

(1) Armand, M.; Tarascon, J. M. *Nature* **2008**, *451*, 652.

(2) Cook, T. R.; Dogutan, D. K.; Reece, S. Y.; Surendranath, Y.; Teets, T. S.; Nocera, D. G. *Chem. Rev.* **2010**, *110*, 6474.

(3) Steele, B. C. H.; Heinzel, A. *Nature* **2001**, *414*, 345.

(4) Rossmeisl, J.; Qu, Z. W.; Zhu, H.; Kroes, G. J.; Norskov, J. K. *J. Electroanal. Chem.* **2007**, *607*, 83.

(5) Koper, M. T. M. *J. Electroanal. Chem.* **2011**, *660*, 254.

(6) Tueysuez, H.; Hwang, Y. J.; Khan, S. B.; Asiri, A. M.; Yang, P. *Nano Res.* **2013**, *6*, 47.

(7) Liang, Y.; Li, Y.; Wang, H.; Zhou, J.; Wang, J.; Regier, T.; Dai, H. *Nat. Mater.* **2011**, *10*, 780.

(8) Jiao, F.; Frei, H. *Angew. Chem., Int. Ed.* **2009**, *48*, 1841.

(9) Xie, X. W.; Li, Y.; Liu, Z. Q.; Haruta, M.; Shen, W. J. *Nature* **2009**, *458*, 746.

(10) Li, Y.; Shen, W. *Chem. Soc. Rev.* **2014**, *43*, 1543.

(11) Xiao, J.; Kuang, Q.; Yang, S.; Xiao, F.; Wang, S.; Guo, L. *Sci. Rep.* **2013**, *3*, 2300.

(12) Hu, L.; Sun, K.; Peng, Q.; Xu, B.; Li, Y. *Nano Res.* **2010**, *3*, 363.

(13) Ma, C. Y.; Mu, Z.; Li, J. J.; Jin, Y. G.; Cheng, J.; Lu, G. Q.; Hao, Z. P.; Qiao, S. Z. *J. Am. Chem. Soc.* **2010**, *132*, 2608.

(14) Risch, M.; Khare, V.; Zaharieva, I.; Gerencser, L.; Chernev, P.; Dau, H. *J. Am. Chem. Soc.* **2009**, *131*, 6936.

(15) Cobo, S.; Heidkamp, J.; Jacques, P.-A.; Fize, J.; Fourmond, V.; Guetaz, L.; Jousselme, B.; Ivanova, V.; Dau, H.; Palacin, S.; Fontecave, M.; Artero, V. *Nat. Mater.* **2012**, *11*, 802.

(16) Surendranath, Y.; Kanan, M. W.; Nocera, D. G. *J. Am. Chem. Soc.* **2010**, *132*, 16501.

(17) Kanan, M. W.; Yano, J.; Surendranath, Y.; Dinca, M.; Yachandra, V. K.; Nocera, D. G. *J. Am. Chem. Soc.* **2010**, *132*, 13692.

(18) Suntivich, J.; May, K. J.; Gasteiger, H. A.; Goodenough, J. B.; Shao-Horn, Y. *Science* **2011**, *334*, 1383.

(19) Mueller, D. N.; Machala, M. L.; Bluhm, H.; Chueh, W. C. *Nat. Commun.* **2015**, *6*, 6097.

(20) Grimaud, A.; May, K. J.; Carlton, C. E.; Lee, Y.-L.; Risch, M.; Hong, W. T.; Zhou, J.; Shao-Horn, Y. *Nat. Commun.* **2013**, *4*, 2439.

(21) Maitra, U.; Naidu, B. S.; Govindaraj, A.; Rao, C. N. R. *Proc. Natl. Acad. Sci. U. S. A.* **2013**, *110*, 11704.

(22) Maiyalagan, T.; Jarvis, K. A.; Therese, S.; Ferreira, P. J.; Manthiram, A. *Nat. Commun.* **2014**, *5*, 4949.

(23) Bajdich, M.; Garcia-Mota, M.; Vojvodic, A.; Norskov, J. K.; Bell, A. T. *J. Am. Chem. Soc.* **2013**, *135*, 13521.

(24) Song, K.; Cho, E.; Kang, Y.-M. *ACS Catal.* **2015**, *5*, 5116.

(25) Kim, T. W.; Woo, M. A.; Regis, M.; Choi, K.-S. *J. Phys. Chem. Lett.* **2014**, *5*, 2370.

(26) Zhang, Y.; Ding, F.; Deng, C.; Zhen, S.; Li, X.; Xue, Y.; Yan, Y.-M.; Sun, K. *Catal. Commun.* **2015**, *67*, 78.

(27) Palmas, S.; Ferrara, F.; Vacca, A.; Mascia, M.; Polcaro, A. M. *Electrochim. Acta* **2007**, *53*, 400.

(28) Nkeng, P.; Poillerat, G.; Koenig, J. F.; Chartier, P.; Lefez, B.; Lopitaux, J.; Lenglet, M. *J. Electrochem. Soc.* **1995**, *142*, 1777.

(29) Belova, I. D.; Roginskaya, Y. E.; Shifrina, R. R.; Gagarin, S. G.; Plekhanov, Y. V.; Venevtsev, Y. N. *Solid State Commun.* **1983**, *47*, 577.

(30) Bockris, J. O.; Otagawa, T. *J. Phys. Chem.* **1983**, *87*, 2960.

(31) Su, H.-Y.; Gorlin, Y.; Man, I. C.; Calle-Vallejo, F.; Norskov, J. K.; Jaramillo, T. F.; Rossmeisl. *Phys. Chem. Chem. Phys.* **2012**, *14*, 14010.

(32) Surendranath, Y.; Nocera, D. G. In *Progress in Inorganic Chemistry*; John Wiley & Sons, Inc.: Hoboken, NJ, 2011; p 505.

(33) Doyle, R. L.; Lyons, M. E. G. *J. Electrochem. Soc.* **2013**, *160*, H142.

(34) Lyons, M. E. G.; Brandon, M. P. *J. Electroanal. Chem.* **2009**, *631*, 62.

(35) Lian, K. K.; Kirk, D. W.; Thorpe, S. J. *J. Electrochem. Soc.* **1995**, *142*, 4309.

(36) Castro, E. B.; Gervasi, C. A.; Vilche, J. R. *J. Appl. Electrochem.* **1998**, *28*, 835.

(37) Tung, C.-W.; Hsu, Y.-Y.; Shen, Y.-P.; Zheng, Y.; Chan, T.-S.; Sheu, H.-S.; Cheng, Y.-C.; Chen, H. M. *Nat. Commun.* **2015**, *6*, 8106.

(38) Trotochaud, L.; Ranney, J. K.; Williams, K. N.; Boettcher, S. W. *J. Am. Chem. Soc.* **2012**, *134*, 17253.

(39) Risch, M.; Ringleb, F.; Khare, V.; Chernev, P.; Zaharieva, I.; Dau, H. *J. Phys. Conf. Ser.* **2009**, *190*, 012167.

DOI: 10.1021/jacs.5b10525
J. Am. Chem. Soc. 2016, 138, 36−39